ISSN 1063-7761, Journal of Experimental and Theoretical Physics, 2007, Vol. 105, No. 1, pp. 99–104. © Pleiades Publishing, Inc., 2007.
Original Russian Text © A.P. Menushenkov, R.V. Chernikov, V.V. Sidorov, K.V. Klementiev, P.A. Alekseev, A.V. Rybina, 2007, published in Zhurnal Éksperimental'noĭ i Teoreticheskoĭ Fiziki, 2007, Vol. 132, No. 1, pp. 114–120.

LOW-TEMPERATURE SOLID-STATE PHYSICS

Low Temperature Features of the Local Structure of $Sm_{1-x}Y_xS$

A. P. Menushenkov[a], R. V. Chernikov[a], V. V. Sidorov[a], K. V. Klementiev[b], P. A. Alekseev[c], and A. V. Rybina[c]

[a] *Moscow Engineering Physics Institute (State University), Moscow, 115409 Russia*

[b] *HASYLAB, DESY, Hamburg, D-22607 Germany*

[c] *Russian Research Centre Kurchatov Institute, Moscow, 123182 Russia*

e-mail: menushen@htsc.mephi.ru

Abstract—The particular features of the local electronic and local crystal structures of the mixed-valence compound $Sm_{1-x}Y_xS$ are studied by the XAFS spectroscopy methods in the temperature range 20–300 K for the yttrium concentration $x = 0.17$, 0.25, 0.33, and 0.45. The temperature behavior of the valence of Sm, as well as of the lengths and the Debye–Waller factors of the bonds Sm–S, Sm–Sm(Y), Y–S, and Y–Sm(Y), has been determined. The violation of the Vegard law has been observed. A model for the estimation of the energy width of the 4*f* level and of its position with respect to the Fermi level is proposed.

PACS numbers: 61.10.Ht, 71.28.+d

DOI: 10.1134/S1063776107070217

The first-order semiconductor–metal isostructural phase transition that occurs at room temperature in SmS under the pressure 0.65 GPa [1] continues to attract close attention of researchers. Under normal pressure, SmS is a nonmagnetic semiconductor with the lattice of the NaCl type. In a semiconductor, "black," phase, the valence of Sm is 2+. However, as the pressure increases and, correspondingly, the volume of the unit cell decreases, the 4*f* level overlaps with the 5*d* band, the bandgap becomes zero, and the transition to a metal, "gold," phase occurs. In this case, because the 4*f* electrons are partially delocalized, the degree of occupation of the 4*f* level becomes noninteger, and samarium passes to a mixed-valence state.

A similar effect in SmS can also be achieved by chemical compression that is created upon replacement of samarium ions by other smaller radius rare-earth or transition-metal ions (Y^{3+}, Yb^{3+}, Gd^{3+}, etc.). At the same time, the above-described phase transition cannot be initiated by introducing divalent ions, such as, e.g., Ca^{2+} [2]. It is likely that, due to electron doping of the 5*d* band, the rearrangement of the electronic structure caused by the replacement of Sm^{2+} with trivalent ions is more complex than that produced by the external pressure. To elucidate the nature of the mixed-valence state and to clarify the effects of doping, dopant concentration, and temperature on the particular features of the local electronic and local crystal structures of $Sm_{1-x}Y_xS$, as well as to determine the interrelation between the valence of the samarium ion and the parameters of its local environment, we applied the X-ray absorption near-edge structure (XANES) technique in combination with the extended X-ray absorption fine structure (EXAFS) method. The XANES technique is sensitive to the electronic configuration of an absorbing ion and makes it possible to determine its valence, while the EXAFS method yields information on the local atomic structure near an absorbing ion.

The samples with the yttrium content $x = 0.17$ and 0.33 were prepared at the Ioffe Physicotechnical Institute, Russian Academy of Sciences (St. Petersburg, Russia), while the samples with $x = 0.25$ and 0.45 were prepared at Tohoku University (Sendai, Japan).

The X-ray absorption spectra of $Sm_{1-x}Y_xS$ were measured over the temperature range 20–300 K above the Sm L_{III} and Y K absorption edges at the beamlines E4 and A1 of the HASYLAB synchrotron center (DESY, Germany). The spectra were processed in the VIPER software environment [3].

Figure 1 presents the EXAFS function $\chi(k)k^2$ obtained from the EXAFS spectrum of a sample of $Sm_{1-x}Y_xS$ with $x = 0.33$ measured at $T = 20$ K above the L_{III} absorption edge of Sm and the modulus of the Fourier transform of this function. To extract the structural information from the spectra obtained, the ranges corresponding to the first (here, Sm–S) and second (Sm–Sm) coordination spheres were selected using a Hanning window. Then, applying an inverse Fourier transform, experimental EXAFS functions corresponding to these coordination spheres in the momentum space were determined. As a result of simulation of these functions, the parameters of the local environ-

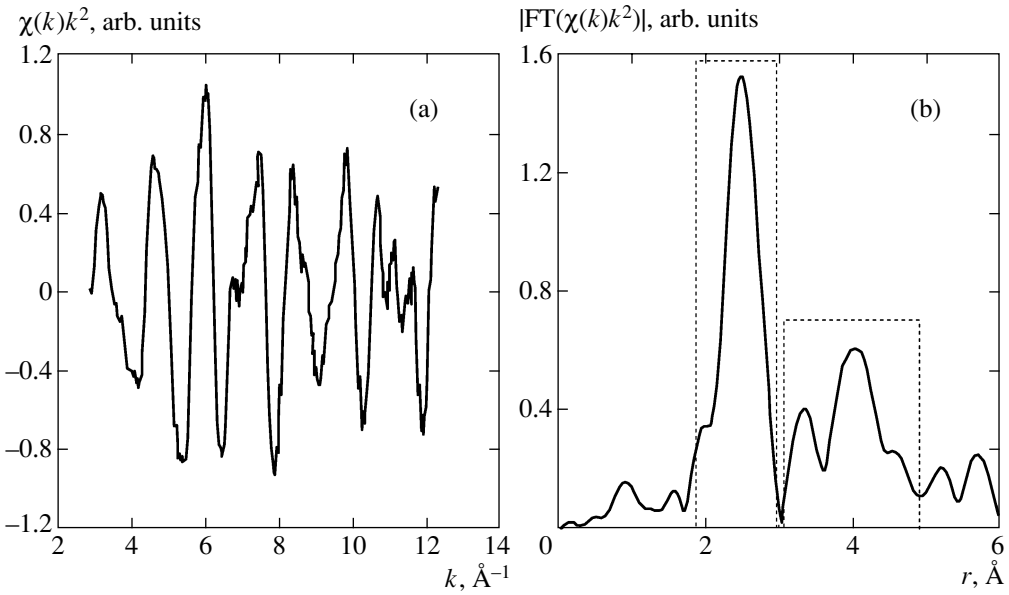

Fig. 1. (a) Experimental EXAFS function $\chi(k)k^2$ measured for a sample with $x = 0.33$ at $T = 20$ K above the L_{III} absorption edge of samarium and (b) modulus of its Fourier transform $|FT(\chi(k)k^2)|$. The rectangles indicate the ranges corresponding to the first (Sm–S) and the second (Sm–Sm) coordination spheres.

ment were extracted. The EXAFS spectra were simulated according to the standard formula

$$\chi(k) = \pm S_0^2 \sum_n \frac{1}{kR_n^2} N_n |f_n(\pi, k)| \times \sin[2kR_n + 2\delta_1(k) + \phi_n(\pi, k)] e^{-2\sigma_n^2 k^2}, \quad (1)$$

where $\chi(k)$ is the EXAFS function; N_n is the coordination number; R_n is the average radius of the nth coordination sphere; and σ_n^2 is the standard deviation of the interatomic distance from its average value, termed the Debye–Waller factor. The scaling factor S_0^2 takes into account many-electron effects. The plus and minus signs pertain to the processing of the L_{III} absorption edge of Sm and K absorption edge of Y, respectively. The amplitudes $|f_n(\pi, k)|$ and the phases $2\delta_1(k) + \phi_n(\pi, k)$ of backward scattering were calculated using the FEFF 8.20 program [4]. Figure 2 shows the experimentally determined and simulated EXAFS functions corresponding to the Sm–S and Sm–Sm spheres of the sample with $x = 0.33$. As a result of simulation, we determined the coordination numbers and found the temperature dependences of the radii and of the Debye–Waller factors for the nearest coordination spheres Sm–S and Sm–Sm(Y), as well as for the spheres Y–S and Y–Sm(Y) (upon measurements above the K absorption edge of Y).

To determine the valence of samarium, we analyzed the fine structure of the spectrum near the L_{III} absorption edge of the samarium atom. For all the compositions investigated, the absorption edge was split into two maxima shifted relative to each other by about 7 eV. This indicates that samarium is in a mixed-valence state, with the average valence of this state being determined by the amplitude ratio of these maxima [5, 6].

The results of the analysis of the XANES spectra are presented in Fig. 3a. It is seen that, at room temperature, the valence of samarium monotonically increases with increasing yttrium content. However, at low temperatures, this monotonicity is violated, and the valence of samarium in the sample with $x = 0.33$ proves to be lower than in the sample with $x = 0.25$. At the same time, the EXAFS data show that the interatomic distances Sm–S and Sm–Sm monotonically decrease with increasing both temperature and yttrium content (see Fig. 3b). This indicates that the Vegard law (the linear dependence of the valence on the lattice parameter) is violated, and, as a consequence, that it is impossible to determine the valence of samarium based only on the measurements of the lattice constant of $Sm_{1-x}Y_xS$ [6]. Most clearly, this violation can be seen on the generalized diagram of the dependence of the interatomic distance Sm–Sm (the lattice constant) on the valence of samarium plotted for the series of temperature measurements from 20 to 300 K performed for all the four compositions (Fig. 4a). Figure 4a demonstrates that the dependence of the lattice parameter on the valence is not only far from linear, but also that it is two-valued: two different values of the lattice parameter in the samples with $x = 0.33$ and 0.25 correspond to one and the same value of the samarium valence. A similar anomaly is also observed in the dependence of the interatomic

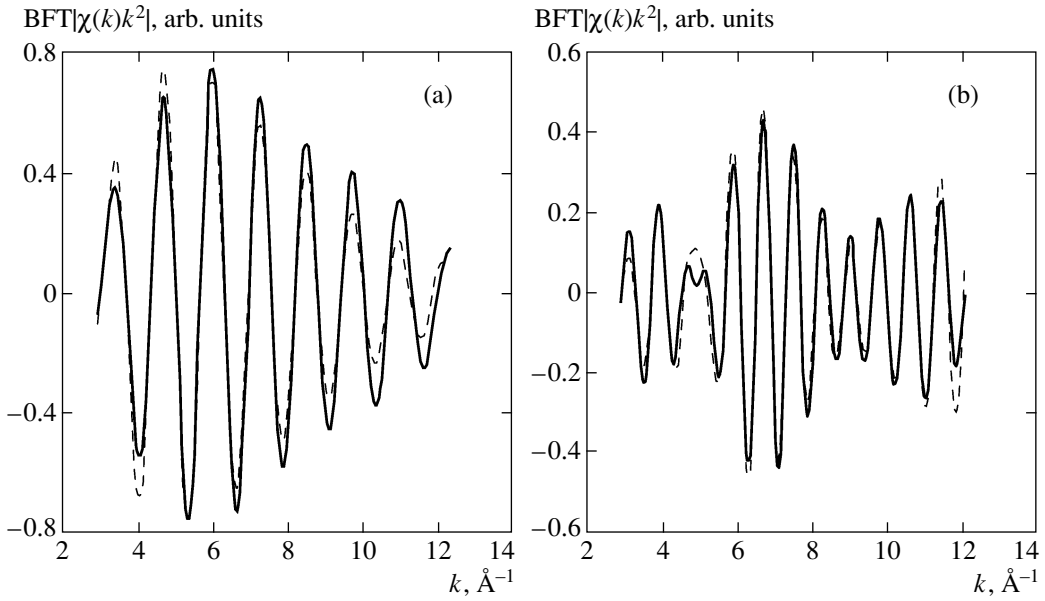

Fig. 2. Experimental (solid curves) and simulated (dashed curves) EXAFS functions $\chi(k)k^2$ corresponding to the (a) first (Sm–S) and (b) second (Sm–Sm) coordination spheres.

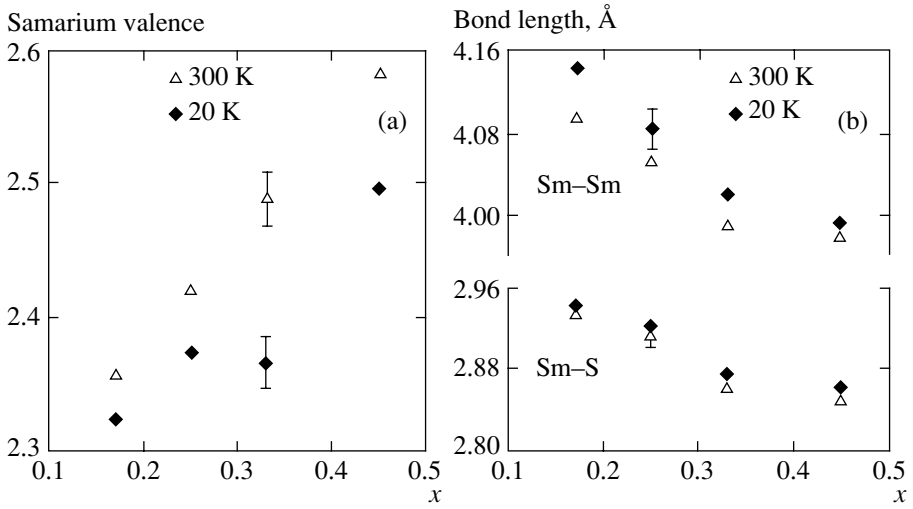

Fig. 3. (a) Samarium valence and (b) Sm–Sm and Sm–S bond lengths measured at $T = 20$ K in relation to the yttrium content.

distance Sm–S on the valence of samarium (Fig. 4b). Since the ionic radius of sulfur remains unchanged, the dependence of the interatomic distance Sm–S describes the relation between the ionic radius and the valence of samarium, whereas the two-valuedness observed means that the ionic radius of samarium ions can acquire different values in different local environments.

The violation of the Vegard law was also observed upon applying pressure to the parent samarium sulfide [7]. According to Varma [8], this effect can be explained by the fact that sulfur ions (cations) "contact" samarium ions (anions) but do not "contact" each other; therefore, anions are subjected to an additional internal pressure. However, the two-valuedness mentioned above has not been observed in undoped SmS. We believe that it is a consequence of an additional electron occupation of the 5*d* band and of the shift of the Fermi level toward higher energies upon doping of SmS with Y^{3+} ions. To illustrate this assumption, we plotted the dependences of the distances Sm–Sm and Sm–S on the total electron occupation of the 5*d* band, n_d, formed by the contributions made by partially delocalized 4*f* electrons of samarium and by *d* electrons of yttrium. These plots are presented in Fig. 5. The total electron occupa-

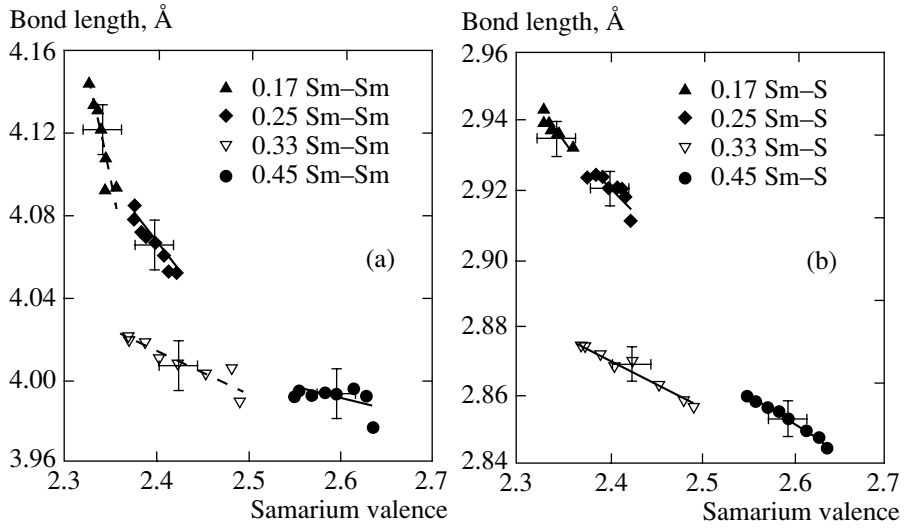

Fig. 4. (a) Sm–Sm and (b) Sm–S bond lengths as functions of the samarium valence measured in the temperature range 20–300 K for samples with different yttrium contents.

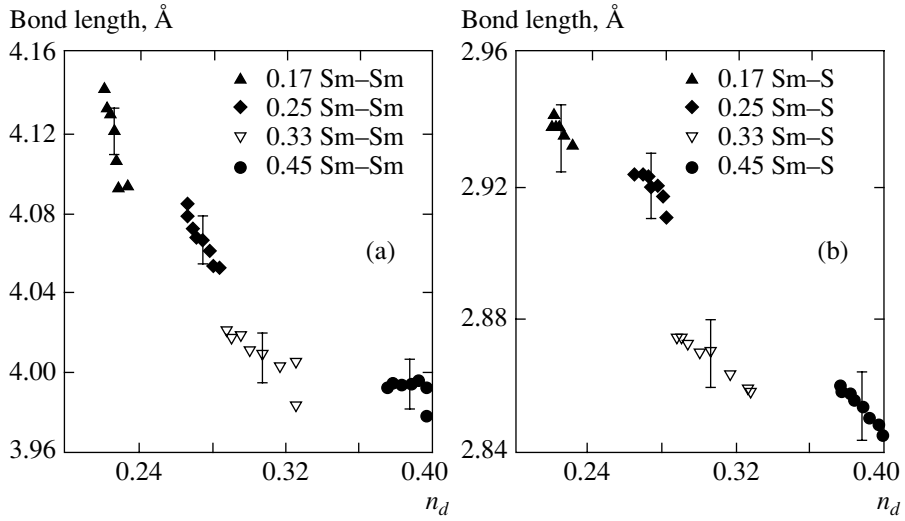

Fig. 5. (a) Sm–Sm and (b) Sm–S bond lengths as functions of the degree of electron occupation of the 5*d* band measured in the temperature range 20–300 K for samples with different yttrium contents.

tion of the 5*d* band was calculated by the formula $n_d = x + (1 - x)(v - 2)$, where x is the yttrium content and v is the samarium valence. As is seen from Fig. 5, the two-valuedness indicated above vanishes; however, the linearity of the dependence of the Sm–Sm and Sm–S distances on the valence of samarium is not restored even if the contribution of *d* electrons of yttrium is taken into account. It is likely that the latter circumstance is connected not only with the internal pressure effect according to the Varma suggestion [8], but also with the local symmetry lowering of the lattice upon doping. Indeed, EXAFS analysis showed that sulfur ions are displaced from their average positions between samarium and yttrium ions toward yttrium ions by distances from 0.13 ($x = 0.17$) to 0.06 Å ($x = 0.45$). This should differently distort the local electronic structure of the compound depending on the yttrium content.

Based on the analysis of the EXAFS spectra, the temperature dependences of the Debye–Waller factors of the bonds Sm–S, Sm–Sm(Y), Y–Sm(Y), and Y–S were also found, which made it possible to determine the Einstein temperatures of these bonds. In X-ray absorption spectroscopy, the Debye–Waller factor of an interatomic distance, equal to the standard deviation of this distance from its average value, is determined by the temperature-independent contribution σ^2, which is caused by the static disorder of atoms, and by the

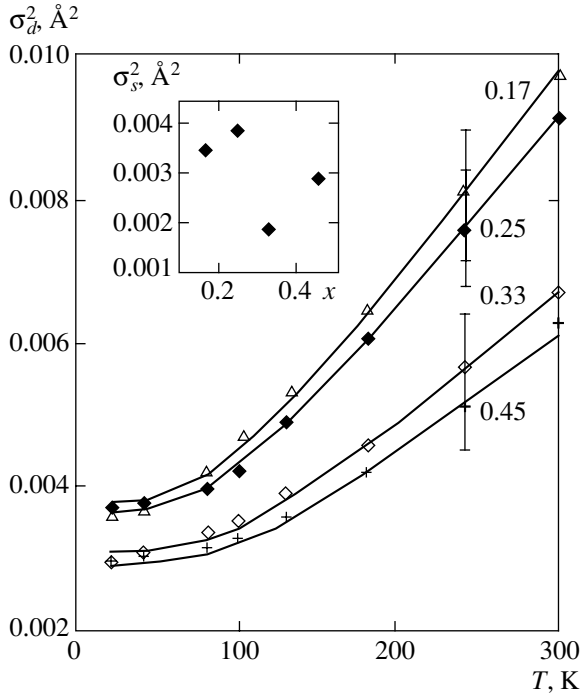

Fig. 6. Temperature dependence of the dynamic contribution σ_d^2 to the Debye–Waller factor of the Sm–S bond. The simulated curves correspond to the temperatures Θ_E (x = 0.17) 243, (x = 0.25) 251, (x = 0.33) 297, and (x = 0.45) 313 K. The inset shows the dependence of the static contribution σ_s^2 to the Debye–Waller factor on the yttrium content.

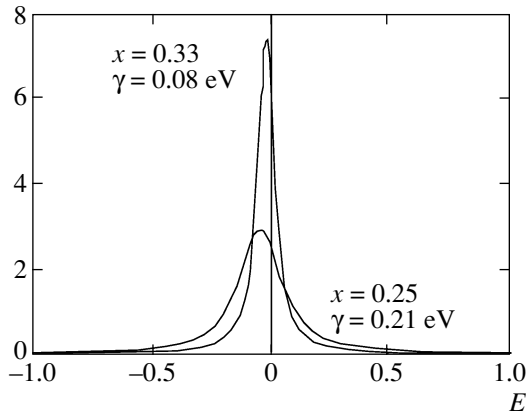

Fig. 7. Simulated functions of the broadening of the 4*f* level of samarium and of the position of this level with respect to the Fermi level for samples with x = 0.25 and 0.33.

dynamic contribution σ_d^2, which characterizes changes in the interatomic distance due to thermal vibrations: $\sigma^2 = \sigma_s^2 + \sigma_d^2$. The temperature dependence of the dynamic contribution can be calculated within the framework of the Einstein model [9],

$$\sigma_d^2 = \frac{\hbar}{2\omega\mu}\coth\frac{\Theta_E}{2T}, \qquad (2)$$

where ω is the frequency of the stretching vibrations of the bond, μ is the reduced mass of the atomic pair; and $\Theta_E = \hbar\omega/k_B$ is the Einstein temperature.

The experimental results along with the simulated curves are presented in Fig. 6. It can be seen that the rigidity of the Sm–S bond, which is characterized by the Einstein temperature, monotonically increases with yttrium content, which is consistent with the decrease in the length of this bond mentioned above. Simultaneously, it was found that the composition with $x = 0.33$ has minimal local static distortions in the crystal lattice, which are characterized by the minimal value of the static Debye–Waller factor of the Sm–S bond (Fig. 6, inset). This circumstance indicates that the degree of ordering in the lattice of $Sm_{1-x}Y_xS$ with the yttrium content $x = 0.33$ is the greatest. It should also be noted that, upon an increase in the temperature from 20 to 300 K, the change in the samarium valence for this composition is the largest (Fig. 3a).

Based on the experimental results obtained, we proposed a model that describes the relation between the valence state of samarium and the local features of the $Sm_{1-x}Y_xS$ lattice and thus determines the main characteristics of the mixed-valence state. Because the valence of samarium depends on the degree of overlap of 4*f* states with free states near the Fermi level, it should depend on both the depth and the width of the 4*f* level. In the most ordered lattice with $x = 0.33$, the broadening of the 4*f* level is homogeneous and is described by the Lorentz function, whereas, for the samples with other concentrations, the broadening of this level is inhomogeneous and is described by the Gauss function (Fig. 7). As a result, as the temperature increases from 20 to 300 K, the same smearing k_BT of the Fermi level E_F causes a different change in the degree of overlap of this level with the 4*f* level and, therefore, in the valence of samarium depending on the depth $\Delta E = E_F - E_0$ and the halfwidth γ of the 4*f* level.

Based on the proposed model and on the experimentally determined temperature dependences of the valence of samarium, we estimated such important characteristics of the mixed-valence state as the depth $\Delta E = E_F - E_0$ and the halfwidth γ of the 4*f* level (see table). The obtained widths of the 4*f* level are of the same order of magnitude as that of the estimate $10^{-2} \le \Gamma_f \le 10^{-1}$ eV of the width of the hybridized *f* band reported in review [8], as well as of more recent theoretical estimates (see, e.g., [10]).

Our investigations showed that the effect of doping on the mixed-valence state in $Sm_{1-x}Y_xS$ cannot be reduced to the effect of chemical pressure alone. A change in the parameters of the local environment of the samarium ion causes an appreciable rearrangement of its electronic structure. The replacement of samar-

Energy depth $\Delta E = E_F - E_0$ and halfwidth γ of the 4*f* level of Sm in $Sm_{1-x}Y_xS$ at $T = 20$ K estimated for samples with different yttrium contents

x	0.17	0.25	0.33	0.45
γ, eV	0.37	0.21	0.08	0.13
ΔE, eV	0.12	0.05	0.02	−0.01

ium ions with yttrium, on the one hand, violates the local symmetry of the lattice of SmS and, on the other hand, affects the valence of samarium, driving it into a mixed-valence state, which additionally contributes to the local deformation of the lattice. The electron doping caused by the replacement of divalent samarium ions with trivalent yttrium ions shifts the Fermi level toward higher energies. This results in a violation of the Vegard law and leads to a two-valuedness in the dependences of the Sm–Sm and Sm–S distances on the valence. The temperature dependence of the valence of samarium is responsible for the anomalous decrease in the lengths of interatomic bonds with temperature, eventually causing a negative coefficient of thermal expansion. A combination of the XANES and EXAFS methods, which provides an opportunity to simultaneously analyze temperature changes in the valence and in local structural distortions, makes it possible to estimate such important parameters of the mixed-valence state as the energy width of the 4*f* level and its position with respect to the Fermi level.

ACKNOWLEDGMENTS

We are grateful to V.N. Lazukov, E.V. Nefedova, and A.V. Kuznetsov for fruitful discussions and to A. Ochiai and A.V. Golubkov for sample preparation. This study was supported by the Russian Foundation for Basic Research (project nos. 05-02-16996 and 05-02-16426).

REFERENCES

1. D. I. Khomskiĭ, Usp. Fiz. Nauk **129**, 443 (1979) [Sov. Phys. Usp. **22**, 879 (1979)].
2. L. D. Finkel'shteĭn, N. N. Efremova, N. I. Lobachevskaya, et al., Fiz. Tverd. Tela (Leningrad) **18**, 3117 (1976) [Sov. Phys. Solid State **18**, 1818 (1976)].
3. K. V. Klementev, J. Phys. D: Appl. Phys. **34**, 209 (2001).
4. A. L. Ankudinov, B. Ravel, J. J. Rehr, and S. D. Conradson, Phys. Rev. B **58**, 7565 (1998).
5. J. Röhler, J. Magn. Magn. Mater. **47–48**, 175 (1985).
6. A. P. Menushenkov, R. V. Chernikov, V. V. Sidorov, et al., Pis'ma Zh. Éksp. Teor. Fiz. **84**, 146 (2006) [JETP Lett. **84**, 119 (2006)].
7. J. Röhler, G. Krill, J.-P. Kappler, et al., in *Valence Instabilities*, Ed. by P. Wachter and H. Boppart (North-Holland, Amsterdam, 1982).
8. C. M. Varma, Rev. Mod. Phys. **48**, 219 (1976).
9. E. Sevillano, H. Meuth, and J. J. Rehr, Phys. Rev. B **20**, 4908 (1979).
10. V. N. Antonov, B. N. Harmon, and A. N. Yaresko, Phys. Rev. B **66**, 165208 (2002).

Translated by V. Rogovoĭ